109
39

THREE-DIMENSIONAL AND OFF-DESIGN STUDIES OF A MACH 7.4 HYPERSONIC INLET

by

Uma Pingali

Thesis submitted to the Faculty of the

Virginia Polytechnic Institute and State University

in partial fulfillment of the requirements for the degree of

Master of Science

in

Mechanical Engineering

APPROVED:

Wing Fai Ng, Chairman

H.L. Moses

E.F. Brown

December 1987

Blacksburg, Virginia

THREE-DIMENSIONAL AND OFF-DESIGN STUDIES OF A MACH 7.4 HYPERSONIC INLET

by

Uma Pingali

Wing-Fai Ng, Chairman

Mechanical Engineering

(ABSTRACT)

In this thesis, three dimensional and off-design calculations were done on a specific Mach 7.4 inlet referred to as the P8 inlet. The Lewis Inlet code was used to obtain numerical results. A few of these results were compared with relevant experimental results obtained from work done at NASA Ames. The three dimensional nature of the flow in the inlet with cut back side plates was studied. This is the first study to be done on the P8 inlet with cut back side plates. It was concluded that though the flow was three dimensional in the inlet, this effect was prominent only close to to the side plates. Hence, a 2-D version of the code could be used to give fairly accurate results and enable a considerable saving of computer time and money. To determine the effectiveness of a hypersonic vehicle at off-design conditions, the code was run with the off-design conditions incorporated in a 2-D run. This was done firstly by changing the angles of attack of the flow in the P8 inlet and secondly by using a different geometry for the inlet i.e. the geometry of the P2 inlet. Conclusions were drawn about the strength of the shock waves at different angles of attack and the mass flow through the inlet for different angles of attack.

ACKNOWLEDGEMENT

I wish to express my gratitude to my guide and mentor, Dr. W. F. Ng. I appreciate his excellent guidance and his accessibility to his students at all times. I thank Dr. E. F. Brown and Dr. H. Moses for consenting to be on my committee. I thank Dr. Norman S. Eiss for his financial support towards the latter part of my graduate study.

I want to express my great admiration and deep gratitude to a lady of exceptional courage and intelligence, my mother. I thank my wonderful husband, Jayaram Sankar, for his invaluable help and moral support all through. I wish to thank all the other members of my family for their love and support .

I also wish to express the debt I owe my Alma Mater, Carmel Convent School, Durgapur, India and my undergraduate school, Indian Institute of Technology, Kharagpur.

Attention Patron:

Page IV omitted from numbering

Table of Contents

List of Illustrations

1. Introduction

The need for swift and efficient transportation has encouraged dramatic improvements in flight technology. The relentless pursuit of excellence has made revolutionary and safe modes of transport accessible to man. Despite the tremendous progress made in this field, the quest for something better is perpetually going on.

Rockets are non air-breathing engines used for flight. They produce very high thrusts but the fuel consumption is excessive and an oxidizer has to be carried on board. Hence rockets are not suitable for long distance flights or cruise missions. Air-breathing turbo-fans and turbo-jets have the capability to assimilate oxygen from the surrounding air and use it for combustion.

Upto a Mach number of about 3, the high thermal efficiency of turbo-jets, fan-jets and prop-jets produces more thrust per unit mass of fuel burnt than other engines. At a Mach number of 3, the turbine inlet temperature (which increases with speed) reaches a maximum permissible value for the material of the aircraft. At speeds greater than Mach 3, the ramjet is used. The ramjet uses the ram air effect to compress the air and eliminates the necessity of a cumbersome rotating compressor.

At speeds above Mach 6, an improvement of the ramjet, called the scramjet, is more effective. While the air in the ramjet falls to subsonic speeds when it enters the combustor, the air enters the scramjet combustor at supersonic speeds and remains supersonic even at the exit from the combustor. Thus, the scramjet produces combustion without slowing the air flow. Because of this, the scramjet has a lower static temperature in the combustor. The lower static temperature ensures lower heat transfer, lower structural loads and greater dissociation of the reaction products. In the range of Mach numbers from 3.5 to 5, the loss of total pressure in the combustor is smaller in the ramjet than the scramjet. This compensates the loss due to a normal shock wave at the inlet of the ramjet. At Mach numbers between 5 and 6, the normal shock losses become too prominent for the ramjet to function [1] . Thus, the scramjet is the only vehicle suited to operate at speeds of Mach 5 and above.

Vehicles operating above the range of Mach 5 are usually considered as hypersonic vehicles. Hypersonic vehicles have extensive application in the military and civilian fields. They are suited to advanced reconnaissance aircraft, accelerator/interceptor aircraft, strategic cruise vehicles and missiles, quick civilian transportation etc. [2,3] . Thus, hypersonic air breathing propulsion is soon becoming a viable proposition.

The inlet plays a very crucial role in hypersonic vehicles. At higher Mach numbers the thrust required is large, thus requiring a large airflow capture. A good design of the inlet enables this requirement to be fulfilled. An annular inlet contiguous with the vehicle's undersurface would be very effective. Today the airframe-integrated scramjet is becoming popular. The unique aspect of this vehicle is the high degree of integration between the structure of the plane and the engine. The forward part of the fuselage forms the surface that provides compression. The rear part of the fuselage acts as the nozzle.

The lower part of the hypersonic inlet consists of a ramp followed by a curved centerbody. The upper body consists of a cowl. The lower surface generates a ramp shock which passes out of the inlet. The cowl generates a cowl shock that gets reflected by the centerbody. Figure 1 shows a schematic representation of the shock structure in the inlet [2] . The vehicle bow shock compresses the flow in the vertical direction.

To enable operation of the inlet over a wide Mach number range, cut back side plates are used. The sweep of the side walls allows spillage to occur effectively in a fixed geometry inlet. The side sweep causes the flow to turn downward and causes spillage ahead of the cowl plate. Thus, the side wall sweep causes the fixed geometry inlet to exhibit a variable geometry like behaviour [4] .

The current aircraft engines for hypersonic speeds form a separate entity from the traditional aircraft structure. In an ordinary aircraft, the engine can be tested separately and then mounted on the aircraft. However for the hypersonic vehicle, since the structural framework forms a part of the engine, the design of the engine and the fuselage are interdependent and it is the combination that should be tested [5] .

The rapid developments in flight technology owe a lot to the progress made in several supporting fields. Today, computational fluid dynamics (CFD) is making an enormous contribution to aeronautical research. The extremely rapid growth in the speed and storage capabilities of the digital computer has enabled CFD to emerge as a very valuable tool in aerodynamic design and analysis. The development of numerical algorithms for the solution of governing equations of fluid motion has further fuelled the growth of CFD [6, 7] . Computers enable evaluation of design configurations and flight conditions that are difficult to test with full size or scaled down models.

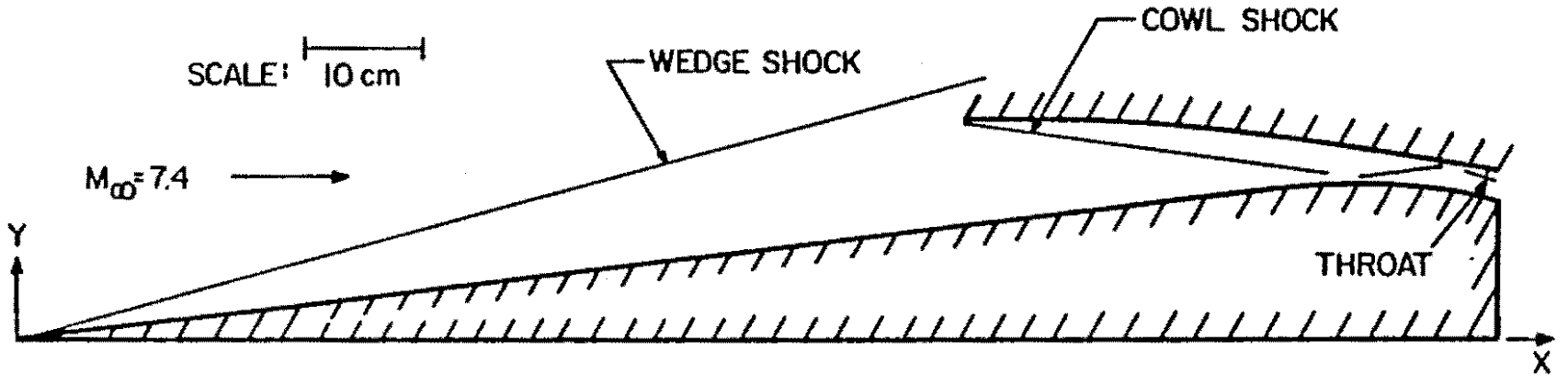

Figure 1. Schematic Representation of the Shock Structure [14]

Combined theoretical and experimental investigation of hypersonic flows are being undertaken. A computer code called Lewis Inlet Code has been developed by NASA to study the complex flows in hypersonic inlets. The flow field in physically realistic situations is three-dimensional, viscous and turbulent. Hypersonic forebody inlet flow fields have complex shock-boundary layer, wedge-boundary layer and shock-shock interactions. The flows interact strongly with thick viscous layers. Because of the complex nature of shock-wave boundary layer interaction it is important to carry out experimental measurements and observations too.

Experiments using scaled down models in a wind tunnel were used to study the hypersonic flow field. The tests were conducted at NASA-Ames [8] . Three different geometries of hypersonic inlets referred to as the P2, P8 and P12 inlets were used in their studies. The P8 and P2 inlet studies are relevant to this thesis. The experiments provided valuable insight into the flow mechanics and also helped to verify the analyses of the Lewis Inlet Code.

Because of the finite width of the wedge and the presence of side plates further downstream, the flow is three-dimensional. This makes the analysis more complicated. To obtain meaningful results from the code a three-dimensional flow analysis may be necessary. This is expected to result in a more accurate and realistic model of the flow.

Design of hypersonic inlets is difficult because of the wide operating range of Mach numbers and angles of attack encountered from take-off to cruise and then to landing. A design that is ideal for cruise is usually unsuitable for take-off and landing. Very often a trade-off is necessary in the various design requirements and the optimum design is to be chosen. Inlet design technology would benefit from a detailed and accurate flow field prediction at off-design conditions too.

The internal compression ratio is the ratio of static pressure at the throat to that at the inlet entrance. The P8 inlet has a compression ratio of 8 and the P2 inlet has a compression ratio of 2. The P2 inlet is suited for acceleration while the P8 inlet is suited for cruise. The forebody results in an external compression ratio of 30 ie. the ratio of static pressure at the entrance to the free stream static pressure was 30. Thus, the overall compression ratio was 60 for the P2 inlet and 240 for the P8 inlet.

Both the inlets have specific geometries that enable these compression ratios to be attained at design conditions. Figure 2 gives a side view of the two inlets to bring out the differences in geometry. The design compression ratio for the P2 inlet was lower than the compression provided by the forebody and cowl shocks. Therefore the internal passage for the P2 inlet had to provide an expanding flow field. The contours of the centerbody and cowl were modified close to the throat to provide slight expansion of the flow field to the design compression ratio.

In this thesis a brief description of the computational code has been given. Important experimental work relevant to this thesis has been enumerated. Important conclusions were drawn about the 3-D nature of the flow and the behaviour of the inlet at off-design conditions.

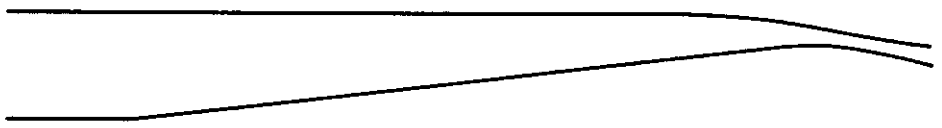

SIDE VIEW OF A P8 INLET PASSAGE

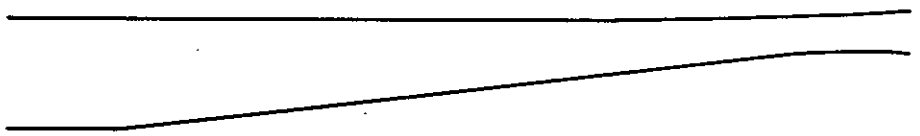

SIDE VIEW OF A P2 INLET PASSAGE

Figure 2. Side View of the P8 and P2 Inlet Internal Passages

2. Background on Application Code

2.1 Introduction

A detailed description of the Lewis Inlet Code has been presented by Buggeln, et. al. [9] and Buggeln, et. al. [10] . However, for the sake of completeness, salient features of the code and a brief outline of the assumptions and equations used in it have been enumerated in this chapter. This helps to provide a general background.

The Lewis Inlet Code is also refered to as the PEPSIS code. PEPSIS is an acronym for ' Parabolic Elliptic Streamwise Implicit Supersonic '[11] . This code solves the set of three dimensional, forward marching equations applicable to flow fields in supersonic inlets. It has been developed to predict the aerodynamics of supersonic inlet systems in general geometries operating at realistic flow conditions.

The computational grid in the given physical domain is generated by an external mesh generator from the coordinates of the upper and lower surfaces of the inlet. An input file is used to specify the boundary layer thickness, the angle of attack, the viscosity model etc. The code has the advantage of being in a modular form such that changes

in boundary conditions, turbulence models or geometry do not cause subroutines and other parts of the code to be changed.

2.2 Assumptions Made in the Code

A number of physically realistic simplifying assumptions are used [10]

1. The Parabolised Navier Stokes Equation, a reduced form of the Navier Stokes Equation, is used.

2. A primary flow direction exists.

3. A coordinate system is constructed with one of its coordinate directions aligned with this primary direction.

4. All diffusion in the primary flow direction can be neglected.

These steps when applied to the steady Navier Stokes Equations produce a set of governing equations that are suitable for the spatial forward marching of supersonic flows. The presence of no slip surfaces along the boundary causes the velocity to become zero at the walls. Hence, outside the supersonic region there is a peripheral subsonic region.

The equations relevant to the code are given in Appendix E. For boundary conditions upstream of the cowl, a technique called the Mach extrapolation technique was used. The concept used is that derivatives of the flow variables in the direction of the Mach angle are small.

3. Experimental Background

3.1 Introduction

Experimental studies with hypersonic inlets were undertaken at NASA Ames to study the flow physics based on which the code could be modeled. Once the code was modeled, these studies also helped to verify the analyses of the code. Details of the experimental work done are available in studies presented by Gos, et. al. [8] and Seebaugh, et. al. [12] . In the 3-D and off-design studies discussed in chapter 4, the results of the code have been compared with some experimental data. For the sake of completeness the experimental work which is relevant to the studies done in this thesis has been briefly outlined in this chapter.

The tests described here were carried out in the Ames 3.5 foot hypersonic wind tunnel at a free stream Mach number of 7.4 and a free stream Reynold's number of $8.86X10^6$ per meter length [8, 11] . A large scale model was used to facilitate easy and accurate measurements. The model used for the experiment had a length of about 127 cm, a forebody length of 81.28 cm, an inlet height of 8.89 cm and an internal passage width

of 35.56 cm. Flow field data survey was conducted at the inlet entrance to determine the entering inviscid and viscous flow. Measurements at many longitudinal locations and at several lateral locations across the entrance and throat were taken.

A wedge forebody was used to simulate the flow field at the entrance of one of the engine modules for the vehicle, thus removing the actual vehicle forebody from consideration in the design of the wind tunnel model. Three internal passages designated P2, P8 and P12 for internal compression ratios 2, 8, 12, respectively, were constructed. The wedge forebody, undercarriage and sting support were common to all internal passages. The interchangeable internal passage sections could be rotated closed for protection of instrumentation during tunnel starting and to vary the contraction ratio to permit inlet starting [12]. Figure 3 gives a schematic representation of the inlet used in the experiments.

Four categories of measurements that are relevant to this thesis are enumerated briefly.

3.2 The Freestream Conditions

The free stream total pressure was measured by a probe located within the settling chamber and by a transducer in the permanent tunnel installation. The pitot pressure was sensed by a pitot tube located at the leading station below the model. The Mach number was determined from the ratio of pitot pressure to total pressure.

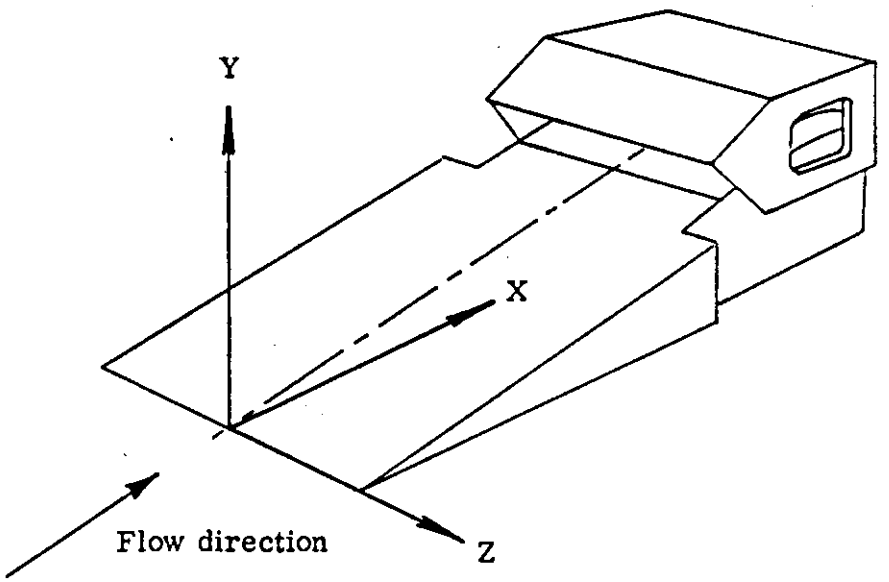

Figure 3. Schematic Representation of the Inlet

3.3 The 2-D Pressure Measurements for the P8 Inlet

Pitot Pressures. Flow properties at desired X locations in the inlet were obtained with probe assemblies traversed vertically during a run. Two rakes, one with pitot pressure and total pressure probes, and the other with static pressure probes were used. For supersonic flows, the pitot pressure measurement is not the actual value in the flow field but the value shown by the pressure gauge because of a shock wave formed at the tip of the probe. An automatic probe drive mechanism with 25 preset stop locations was used to advance the probe assemblies to make flow measurements at .064 cm intervals. These readings were not taken at the centerline in the lateral direction. They were taken at a distance from the centerline equal to .3 of the distance between the centerline and the side plate.

Surface Static Pressures. The surface properties on the centerbody and cowl were also measured during this vertical traversal. Both cowl and centerbody pressures were recorded when the probe assembly was at its maximum distance from the respective surface. This procedure minimized the effects of probe interference on surface pressure readings.

3.4 3-D Measurements

Pitot pressure measurements were taken at several lateral locations at the entrance and throat. At the inlet entrance station the flow field data was obtained at 9 lateral locations as shown in figure 4. Figure 4 also shows the lateral locations along the throat at which data was obtained.

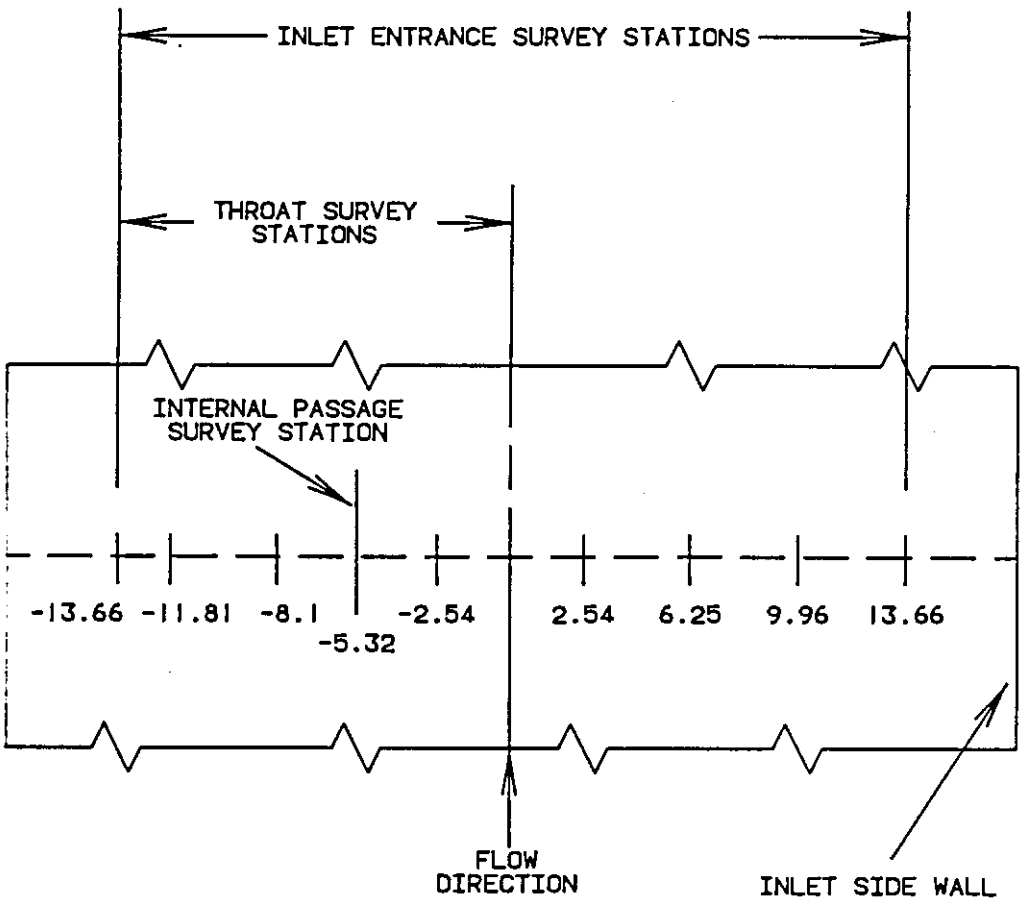

Figure 4. Lateral Survey Stations at the Entrance and Throat

3.5 Off-Design Measurements

P8 Off-Design Measurements. The angle of attack of the wedge forebody was changed from the design value of 6.5 to the overspeed value of 4.5 and underspeed value of 8.5. The overspeed case resulted in an entrance Mach number of 6.3 and the underspeed case gave an entrance Mach number of 5.7. Surface pressures on the cowl and centerbody were recorded.

P2 Measurements. This is the first set of measurements done with the P2 geometry. All the other measurements described above were done on the P8 geometry. In this, a P2 geometry was studied as an off-design case of the P8 inlet. The pitot pressure measurements and the surface static pressure measurements were measured just as was done for the P8 case.

4. Results and Discussion

The results are discussed in the next two sections. Chapter 4.1 discusses the three dimensional effects of the flow. Chapter 4.2 discusses the study with off-design conditions.

4.1 Three-Dimensional studies

4.1.1 Introduction

The important physical components of the inlet are the wedge forebody, inlet centerbody, inlet cowl and two side plates. The three dimensional effect comes into play because of the finite width of the wedge and the presence of side plates. An attempt was made to study the effect of the three dimensionality of the flow on the boundary layer development, shock wave impingement and pressure distribution. The pressure and velocity distribution at different cross sections were studied. For a number of lateral positions, pitot pressure distribution at different streamwise locations were studied to illustrate the three-dimensional nature of the flow. This was compared with the pitot pressure distribution obtained from a 2-D analysis to determine the scope and effectiveness of two-dimensional modeling.

3-D flow studies with the P8 inlet were done at NASA Lewis Research Center [13] . Straight side plates were used in the studies. However, in the research described in this

thesis cut-back side plates were specified in the code. This study done with cut-back side plates is the first of its kind to be done with the Lewis Inlet Code.

4.1.2 Discussion of the Plots

Figures 5 to 9 show the secondary velocity vectors and Mach number contours at various cross sections. Since the flow is symmetrical about the cross section, calculations were done and subsequent plots were shown for only half the inlet. The secondary velocity vectors were plotted for the right half of the cross section, as one looks into the inlet, and the Mach number contours were plotted for the left half. Thus, for both the plots, the ramp surface was on the bottom and the cowl surface was on the top. But the plot for secondary vectors had the side plate on the right hand side while the Mach number contours had the side plate on the left hand side.

The Mach number contours and the secondary velocity vectors yield a lot of information on the boundary layer development and the nature of shock waves present in the inlet. The concentration of Mach contours near a solid surface denotes the presence of boundary layers while a similar concentration away from the solid surface signifies a shock wave. Velocity vectors that abruptly change their direction also show the presence of a shock wave. The size of the arrow head is scaled proportional to the size of the arrow i.e. the magnitude of the velocity vector.

Figure 3 shows the orientation of the co-ordinate system with respect to the inlet. A parameter X/HC is used to specify locations in the primary streamwise direction. X is measured from the leading edge of the ramp and is nondimensionalized by HC, the inlet

capture height. For this inlet, the X/HC values extend from 0 at the centerbody leading edge to 7.1 at the inlet throat.

Figure 5 shows the plots at an X/HC value of 4.4 . This location is just upstream of the cowl. The concentration of Mach contours on the ramp surface shows the presence of a thick boundary layer. There is no concentration of contours away from the solid surface and no sudden change in the direction of the secondary velocity vectors. From this it can inferred that the shock wave passes out of the flow field and does not hit the cowl. The flow in the Z direction is uniform.

Figure 6 shows the plots at an X/HC value 5.72 which is between the cowl and the throat. There is a cowl shock wave moving towards the centerbody. Besides, there is a weak shock moving out away from the side plate. A vortex is being formed where the shock wave glances the boundary layer. It pumps fluid from the cowl boundary layer, down the side plates and on to the ramp surface.

Figure 7 shows the plots at the location where the cowl shock wave impinges on the centerbody. This is at an X/HC value of 6.21. The strong glancing shock boundary layer interaction causes a very strong vortex. It extends beyond just the corner. The effect is felt till about half the distance between the side plate and the centerline. The strong vortex is able to carry fluid along the centerbody to a much farther distance.

One would expect the design of the inlet to be such that the cowl shock wave would get cancelled. However, this does not happen because of the thick boundary layers on the surfaces and the bending of the shock waves near the side plates. Figure 8 shows the plots at X/HC of 6.91 which is where the shock wave reflects off the centerbody and onto the cowl. The boundary layer is very thick at the corner and decreases towards the center. The flow is very non uniform.

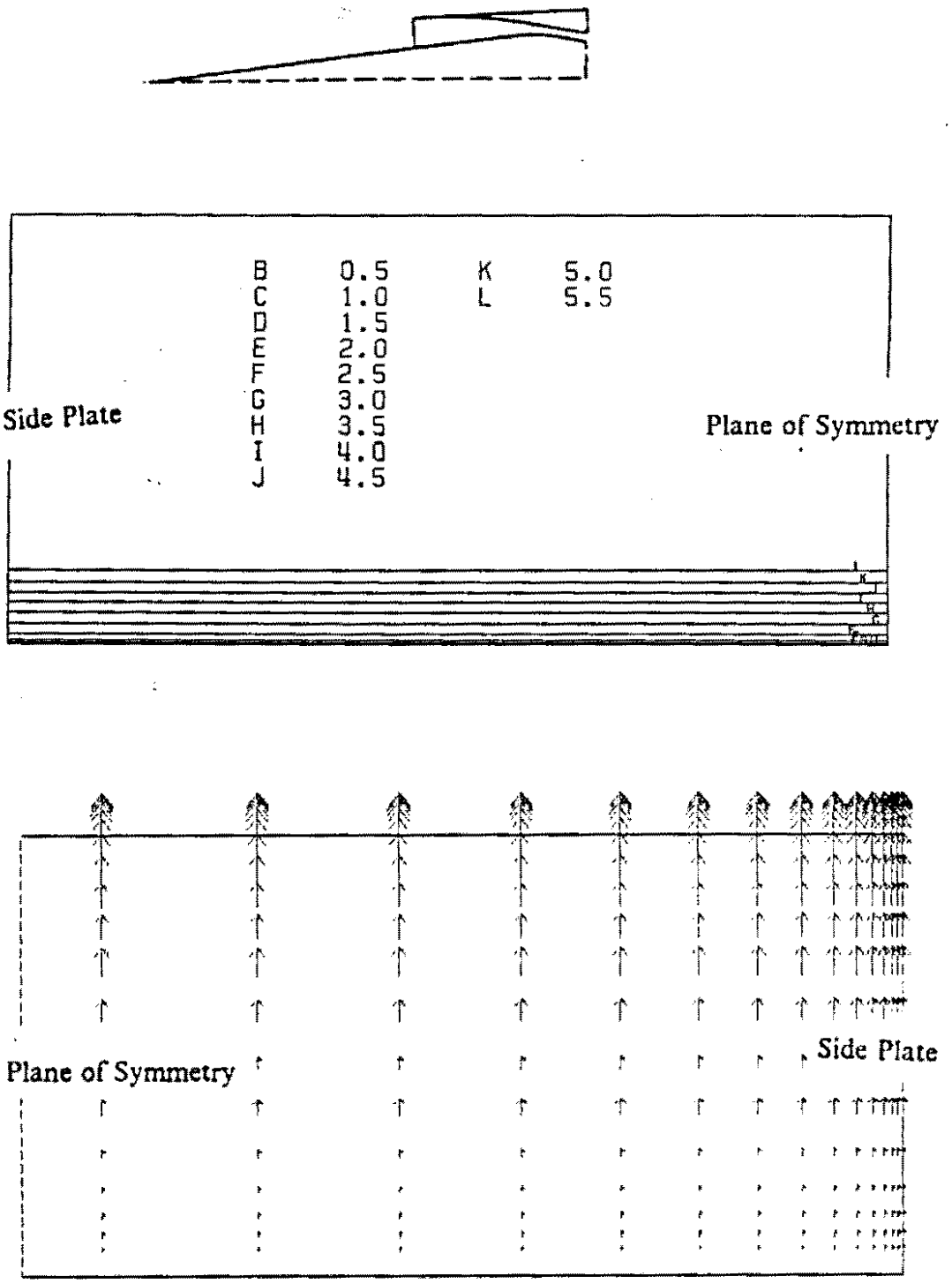

Figure 5. Mach No. Contours and Secondary Velocity Vectors Before Cowl Lip

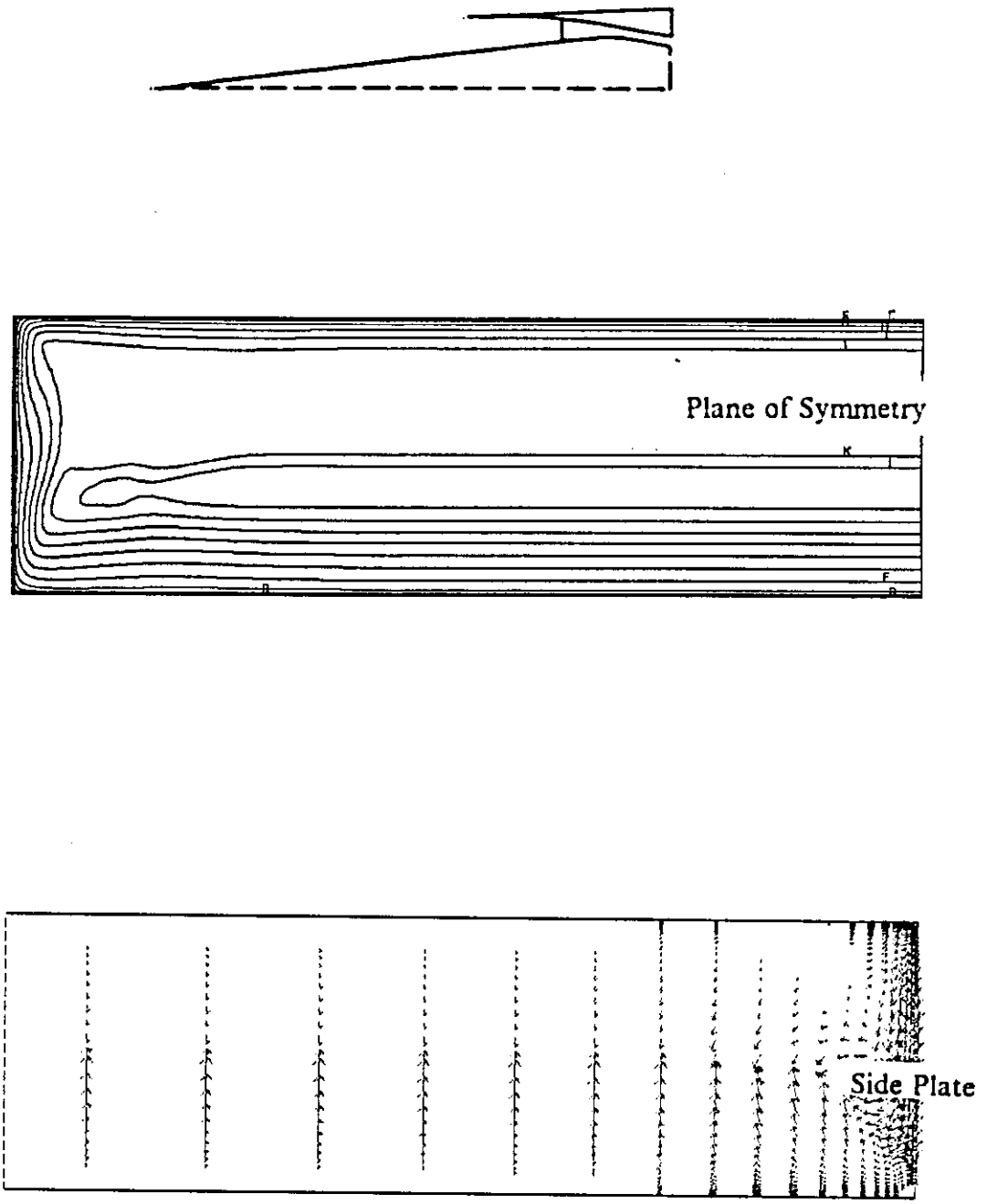

Figure 6. Mach No. Contours and Secondary Velocity Vectors Downstream of Cowl Lip

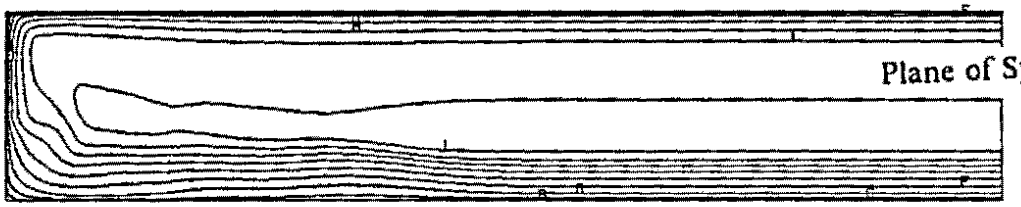

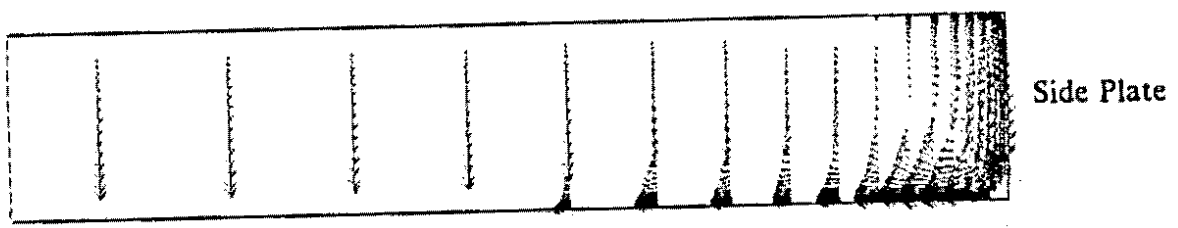

Figure 7. Mach No. Contours and Secondary Velocity Vectors at Centerbody Shock Reflection

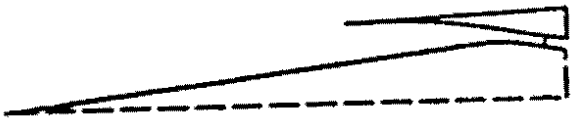

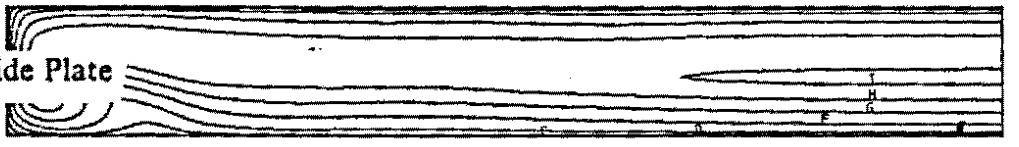

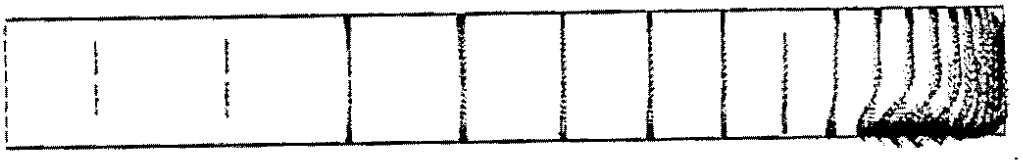

X/HC = 6.91

Figure 8. Mach No. Contours and Secondary Velocity Vectors at Cowl Shock Reflection

Figure 9 shows the plots at X/HC equal to 7.08 which is just at the throat. The vortex is able to pump fluid along the centerbody right upto 75% from the side plate. The shock wave is perceived again in the velocity vectors and the contours. It can be seen that the shock wave is bent across the cross section width.

Figure 10 shows the static pressure contour plots along the XY plane at various Z locations. Four planes were considered

1. The centerline where Z = 0

2. Z = .3, the plane at which the pressure and the temperature probes are placed in the experiment.

3. Z = .5, the plane midway between the side plates and the centerline

4. Z = .75

The plots are shown on a part of the inlet, starting from the cowl lip.

The difference between the shock pattern at Z = 0 and Z = .3 is that as the Z location shifts towards the side plates, the effect of the side plates becomes more pronounced. The cowl shock wave does not change much at the first three locations. But at the fourth location , the shock wave interacts with the boundary layers from the side plate. This causes the point of impingement of the cowl shock on the centerbody to move farther upstream. Thus, this shock wave is less inclined to the ramp surface.

Considering the reflected shock from the centerbody and onto the cowl, as the plane considered shifts towards the side plate the shock wave strikes the cowl farther upstream.

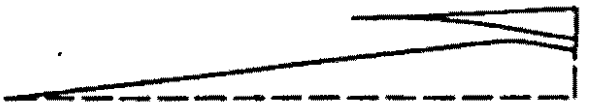

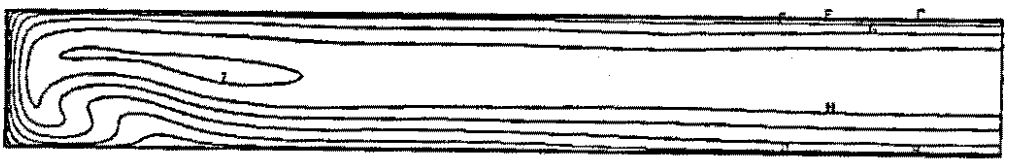

Side Plate

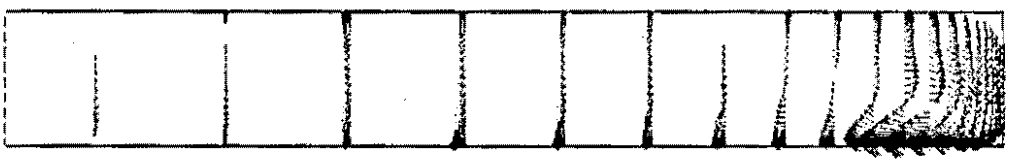

Side Plate

X/HC = 7.08

Figure 9. Mach No. Contours and Secondary Velocity Vectors at the Inlet Exit

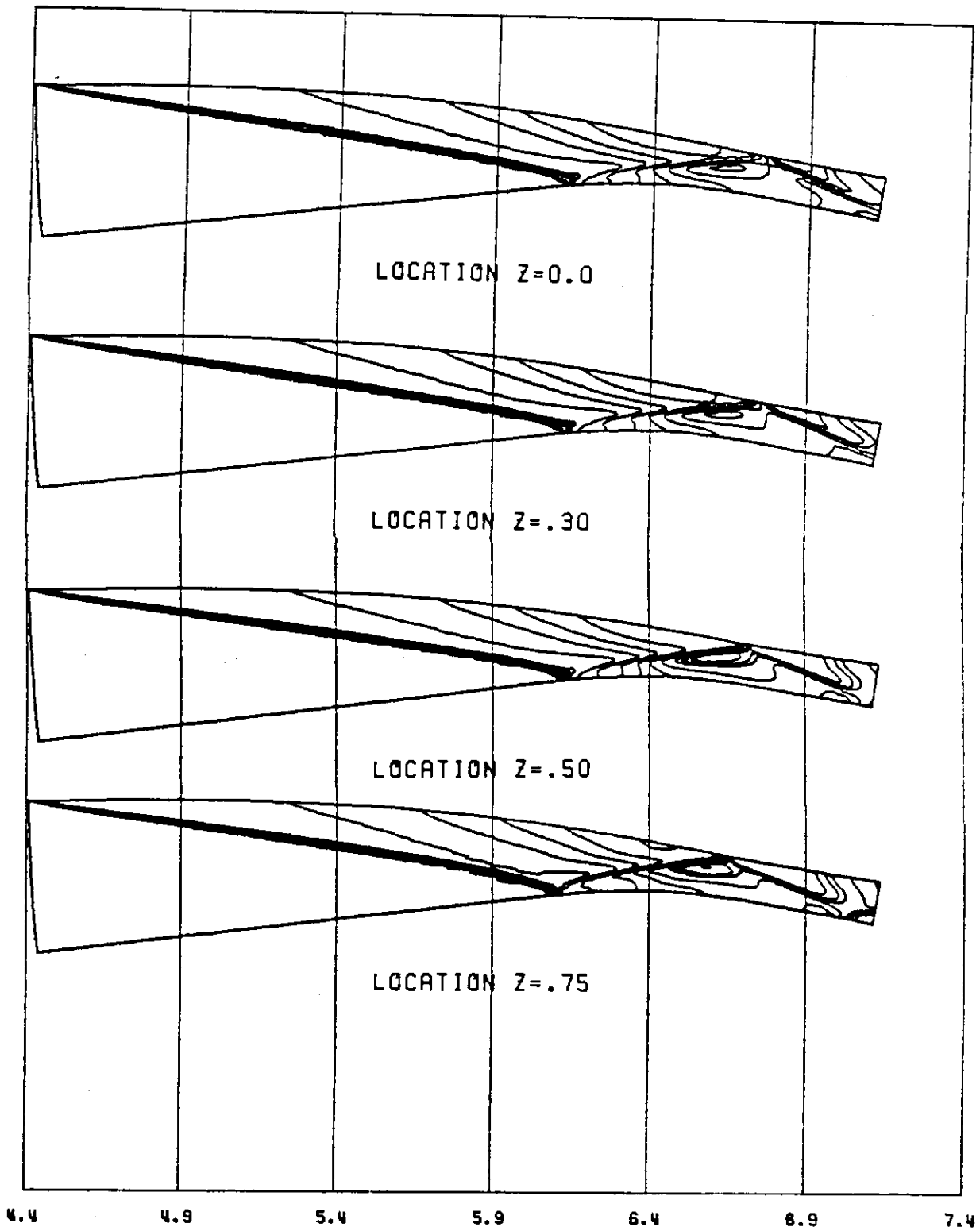

Figure 10. Static Pressure Contours of P8 Inlet at Various Spanwise Locations

For the fourth case, which is close to the side plates, this shock wave is much more inclined than in the other cases.

There is not much of a difference between the first three planes but there is a marked difference in the last one. Thus, the inlet shows a 2-D effect over more than half the inlet in the spanwise direction but 3-D effects become prominent close to the side plates.

Figure 11 shows the cross section of the inlet in the XZ plane. A plot of the centerbody surface and the cowl surface pressures is presented. In both cross sections the centerline is on the lower part and the side plate is on the upper part. The other half of the inlet is just a mirror image of this about the centerline.

From the centerbody pressure plot, the point of impingement of the first cowl shock can be gauged as the first point of concentration of the contours. However, this effect spans over only about 40% of the width. Thus, the effect is mainly two dimensional. However, further downstream when the next impingement of the cowl shock takes place the next concentration of contours spans almost the whole width of the inlet. In both cases, after the shock impingement, there is a high pressure region formed away from the centerline.

The cowl pressure distribution in turn shows a great interaction of the side plate boundary layer with the cowl shock.The centerbody shock impingement effected the cowl similar to how the cowl shock impingement effected the centerbody.

On comparing Figures 5 to 11 with similar figures obtained at the NASA Lewis Center with straight side plates [13] no significant differences were observed in the velocity vector and Mach number contours. However, flow physics predicts a difference between the flow fields in an inlet with straight side plates and cut back side plates. Though the

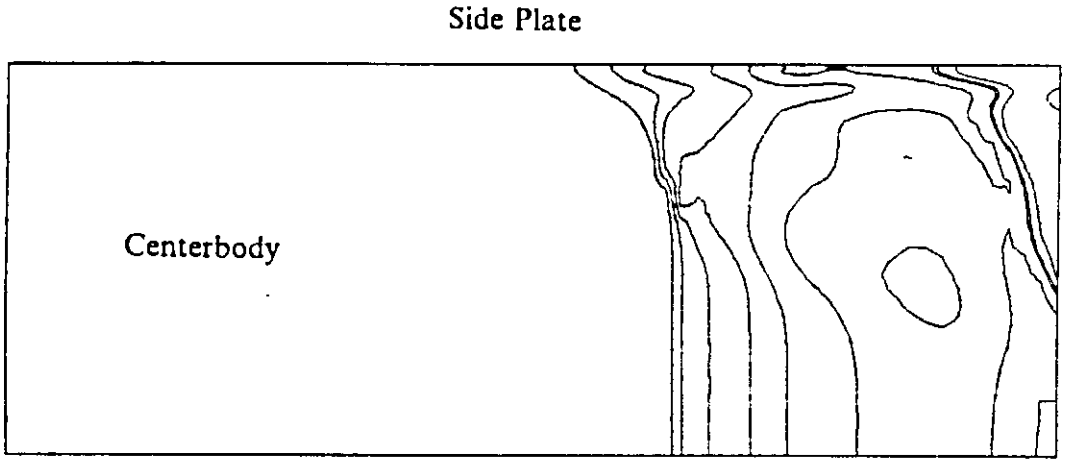

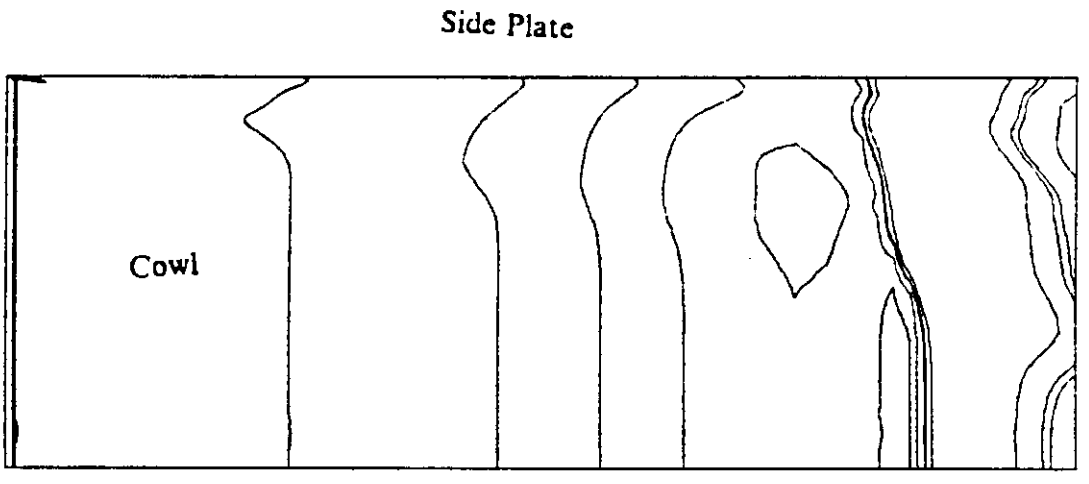

Figure 11. Surface Static Pressure Distributions on the Centerbody and the Cowl

code models the side plates accurately, the code does not bring out the difference between the cut back and straight side plates because the wedge was modeled as an infinite wedge. In the experiment, the wedge had a finite width which acted with the side plates to bring in additional 3-D effects. Thus, the actual flow field with cut back side plates is not completely represented with the limitations of the present code. The infinite wedge model however has applications in the proposed futuristic multiple module inlets.

Figure 12 shows the comparison of the experimental data with the 3-D calculated values at Z=0 and at Z=.3. Z=.3 is the lateral location where the experimental values are recorded.

The pitot pressure plots show the pitot pressure values along the vertical direction for a number of locations in the streamwise direction. The circles represent the values obtained from experiments. The light line shows the calculated values at the survey lateral plane and the dark line shows the calculated values at the centerline. Y=0. corresponds to the centerbody and the uppermost point corresponds to the cowl surface. The presence of the boundary layer and its thickness can be gauged by the profile of the pitot pressure close to the centerbody and the cowl. The more inclined these profiles are to the horizontal direction, the thicker are the boundary layers at the two surfaces. The location of an impinging shock wave is clearly identified by the abrupt increase in pitot pressure. As the shock wave penetrates the centerbody boundary layer, the wave location becomes more difficult to identify. Where abrupt pressure rises are not evident in the boundary layer region, the wave location can be identified from changes in slope or small discontinuities in profiles. For location X/R = 6.32 and locations further downstream, the abrupt change in pitot pressure indicates the location of reflected shock. The low pitot pressure in the vicinity of this is due to an expansion region upstream of the reflected wave.

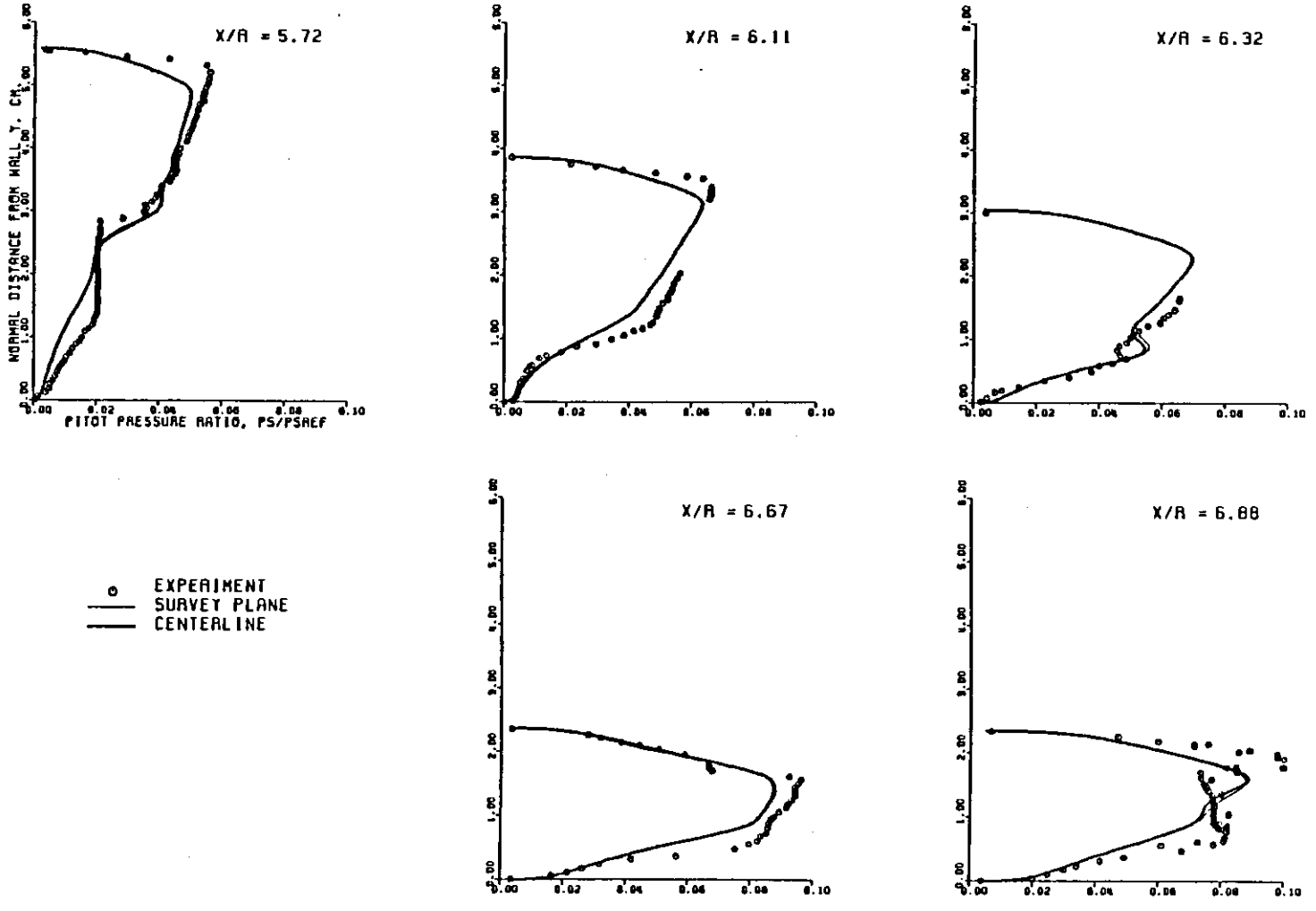

Figure 12. Comparison of Centerline and Survey Plane Pitot Pressure Distributions from the code with Experimental results.

The pitot pressure plots of the two locations overlap. Thus, the flow field is 2-D between the centerline and the survey plane.

4.1.3 Comparison with the 2-D Run

A 2-D version of the code was executed using exactly the same input file as the 3-D run except for the 2-D option. The 2-D version of the Lewis Inlet Code uses the centerline plane. Figure 13 shows the pitot pressure plots of the 2-D run compared with the the 3-D plots at the spanwise survey location. The distance of this plane from the centerline is .3 of the distance between the centerline and the side plate . The dark line shows the results from the 3-D analysis and the light line shows the results from the 2-D analysis. The experimental values are also shown on the same plot. The 3-D run used 100 points in the Y direction and 60 points in the Z direction. 2170 steps were used in the X direction. The 2-D run used 100 points in the Y direction. 960 steps were used in the X direction. The two pitot pressure plots overlap .

A very good match was obtained between the 2-D and the 3-D case. Thus, instead of using the 3-D calculations at the survey plane, the 2-D calculations can be used without much loss of accuracy. The 3-D flow calculations and graphical representations showed that the 3-D effect was very significant in the hypersonic inlet. However, this effect became noticeable only close to the side walls. Over most of the inlet the flow was 2-D . Hence to determine the response of the inlet to off-design conditions, the 2-D option was used. A considerable saving of computer time and money could be achieved. The 3-D run used a CPU time of 18.3 seconds per station in the X direction. The CPU time used by the 2-D run was about .001 of this time. Physically, since the fuselage maximum

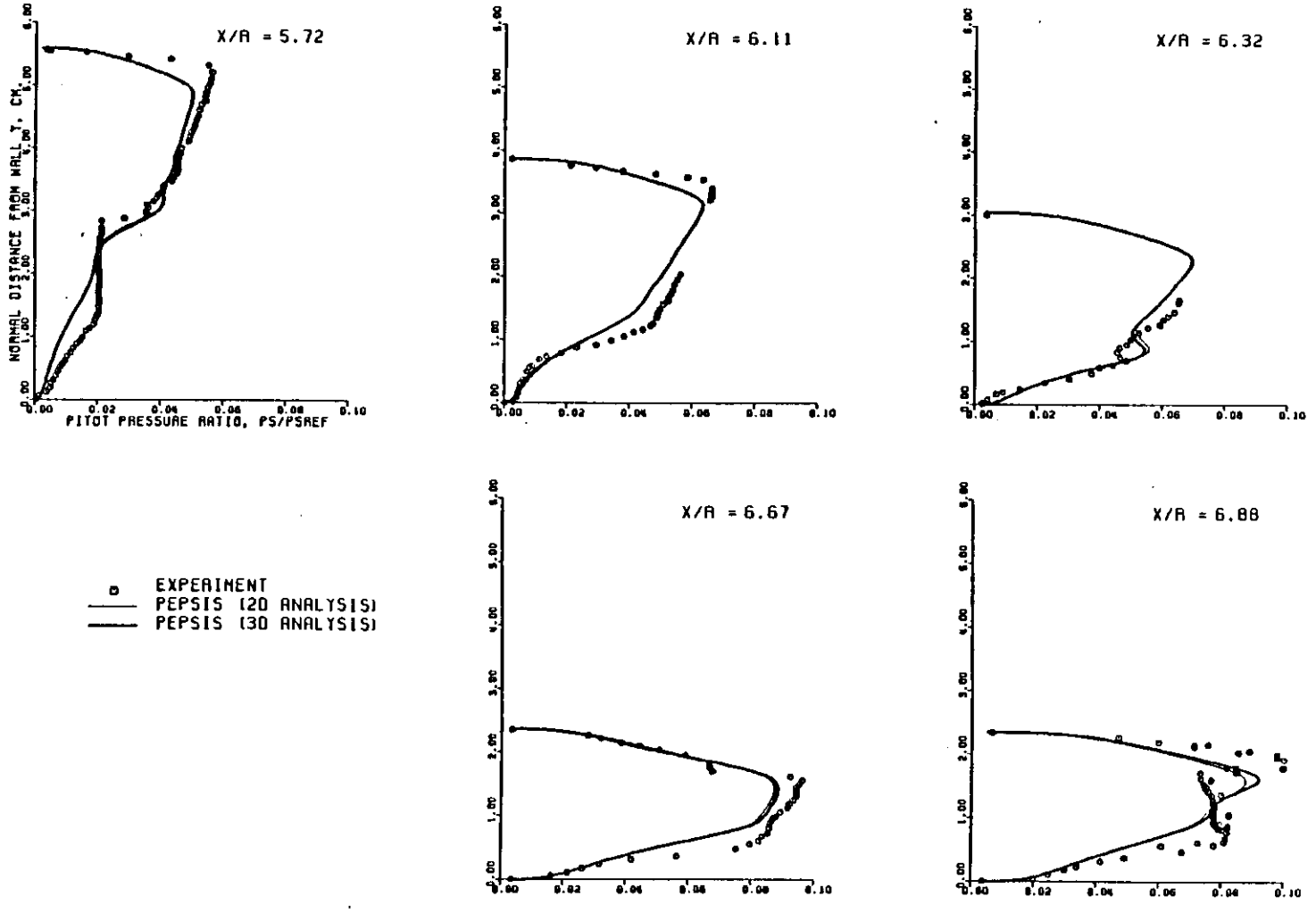

Figure 13. Comparison of 2-D and 3-D Pitot Pressure Distributions with experimental results.

diameter is large relative to the engine module height, the flow at the inlet entrance and within the internal passage is nearly two dimensional [8] .

In the studies done by Kumud [14] it was shown that the best modeling of the flow in the P8 inlet was obtained when transition from laminar to turbulent flow was taken into consideration on the cowl and centerbody surfaces. To model turbulence, the McDonald Camarata model with the Bushnell Beckwith high speed correction was used for the best comparison with experimental results. The McDonald Camarata model is a method for calculating turbulent boundary layers using an extended mixing length hypothesis to calculate the turbulent shear stress distribution in the boundary layer. The existing implementation of the McDonald Camarata model on the Lewis Inlet Code was modified to account for high speed effects in compressible flows. This gave a significant improvement because the original McDonald Camarata model was developed for incompressible flows only[14] .

However, in this study to keep the 3-D calculations simple, transition was not taken into account. Thus, the boundary layer was considered to be turbulent on both the cowl and centerbody surfaces. Also, the Bushnell Beckwith correction was not incorporated into the McDonald model because it was not yet available for 3-D applications at the time of this study. Despite these limitations, good results were obtained and important conclusions could be made.

4.2 2-D Off-Design Studies

4.2.1 Introduction

The importance of off-design studies has been emphasized in the introduction. This is the first time that the Lewis Inlet Code has been used for off-design studies of the P8 inlet involving angles of attack and different compression ratios. To determine the effectiveness of a hypersonic vehicle at off-design conditions, the code was run with the off-design conditions incorporated in a 2-D run of a P8 inlet. The angles of attack were varied in both the positive (counter-clockwise) and negative (clockwise) directions. A mass flow analysis was done at various angles of attack. The surface pressures of the cowl and centerbody were studied at different angles of attack to analyze shock impingement and shock strength. Pitot pressure contours were plotted to depict the ramp and cowl shock angles.

As another aspect of the off design conditions, a P2 inlet (which had a compression ratio of 2) was studied as a comparison to the P8 case (which had a compression ratio of 8). Different parameters, e.g. the boundary layer thickness on the upper and lower surfaces

were varied till a good match with the P2 experimental data was obtained. These parameters were then compared with those obtained from the study of the P8 inlet.

The McDonald turbulence model with the Bushnell Beckwith correction was used for these off-design studies. 99 points were used in the Y direction and 960 points were used in the X direction.

4.2.2 Angle of Attack Studies on the P8 Inlet

1.Comparison of the results of the +2 deg and -2 deg angles of attack with the experimental results.: As outlined in Chapter 3, some data about the surface pressures were obtained for two off-design conditions . Figure 14 shows the orientation of the flow for the design condition and the two off-design conditions.

1. The angle of attack of the wedge forebody was kept at 4.5 degrees. Thus for a ramp of 6.5 deg the angle of attack of the air stream was specified as +2 deg with respect to the initial flow direction. The positive angle turned the flow in the counter clockwise direction. This was the overspeed case.

2. The angle of attack of the wedge forebody was kept at 8.5 deg. Thus, for a ramp of 6.5 deg the angle of attack of the air stream was made -2 deg . The negative angle turned the flow in the clockwise direction. This was the under speed case.

At design conditions, the entrace Mach number was 6. At the overspeed condition, the entrance Mach number was 6.3. At the underspeed condition the Mach number was 5.7.

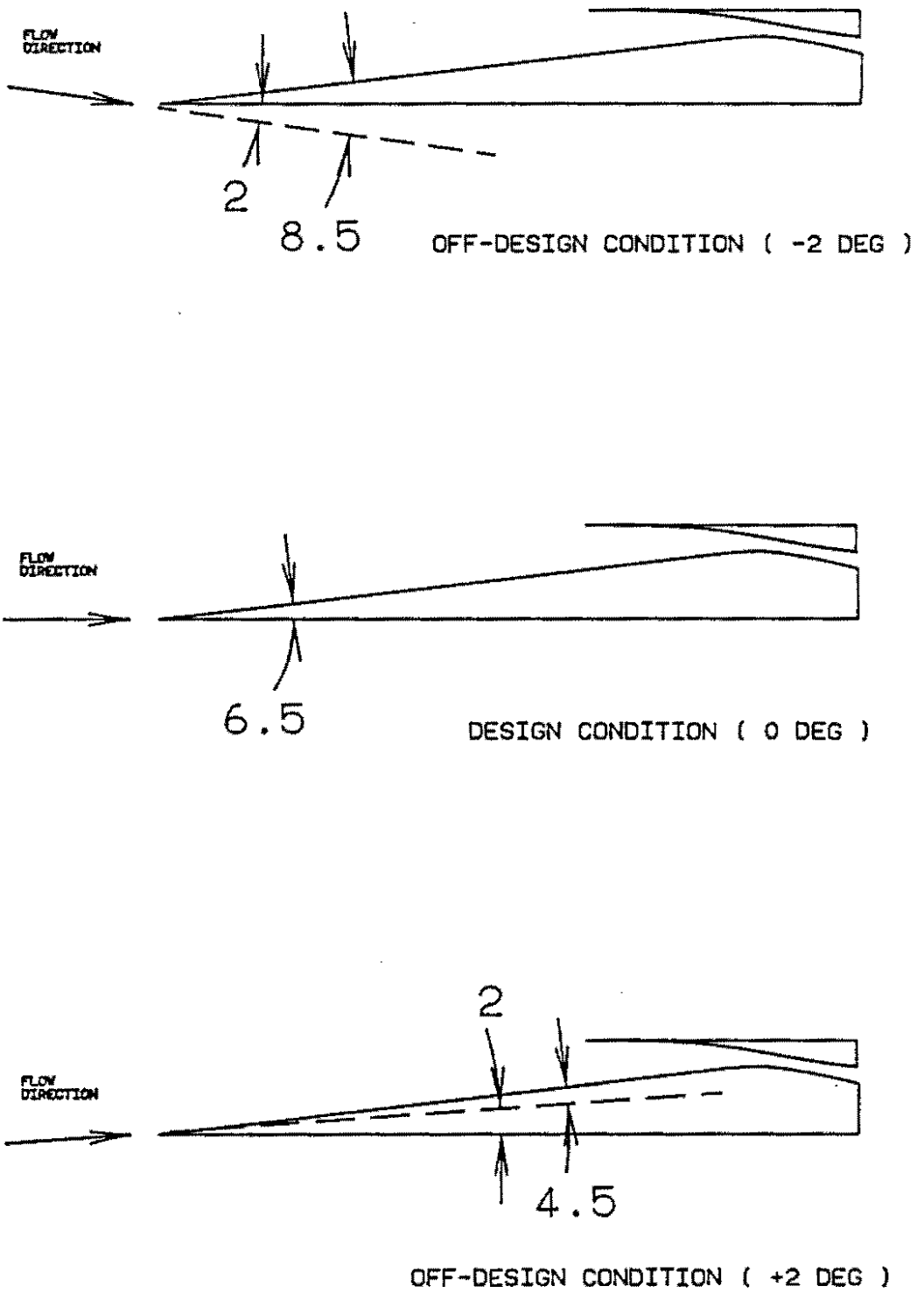

Figure 14. Orientation of the Flow for the Off-Design Study

A listing of the input file of the Lewis Inlet Code is given in Appendix B. Using the parameter ' BETA ' in LIST 4 of the input, values of +2 and -2 were specified for the underspeed and overspeed cases respectively. The experimental data in the off-design surface pressure plots was the relevant data for that particular off-design condition.

An angle of attack of +2 deg gave an entrance Mach number of 5.7 and an angle of attack of -2 deg gave an entrance Mach number of 6.3. The surface pressures on the cowl and centerbody are shown in Figure 15. It is seen that the profiles match very well with the experimental data.

On the centerbody static pressure plot, the sudden increase in pressure at location 6.2 is due to the cowl shock interacting with the centerbody boundary layer. On the cowl static pressure plot, the drop in pressure around the location 6.5 is due to the expansion wave that develops as the cowl shock enters the centerbody boundary layer. Beyond this region, the increase in pressure was due to the interaction of the reflected shock wave with the cowl boundary layer.

The good match with the experiment showed that the code was suited to study off-design conditions.

2. Results of Mass Flow Calculations The method used for mass flow calculations is given in Appendix D. The following important results were obtained.: The inlet capture mass is the mass that goes through the internal passage between the cowl and the centerbody.

Centerbody

Cowl

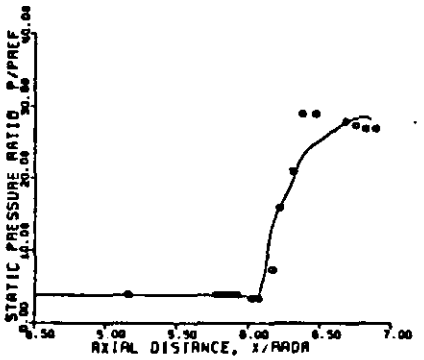

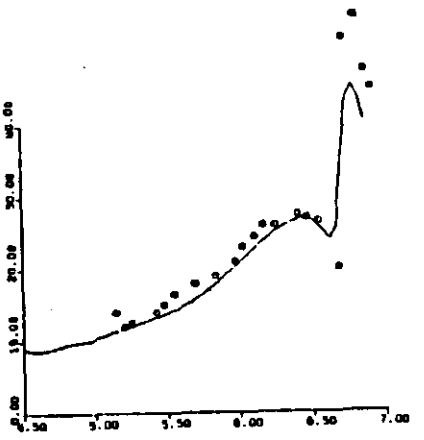

Angle of Attack = -2°

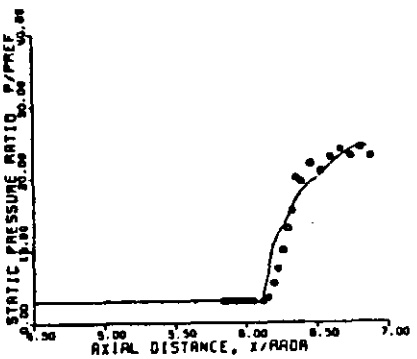

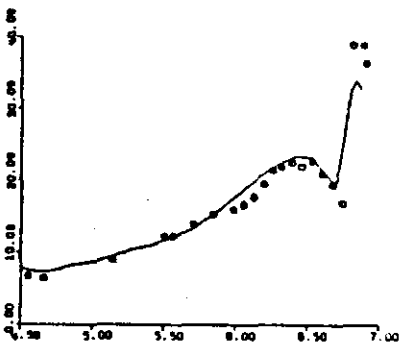

Angle of Attack = 0°

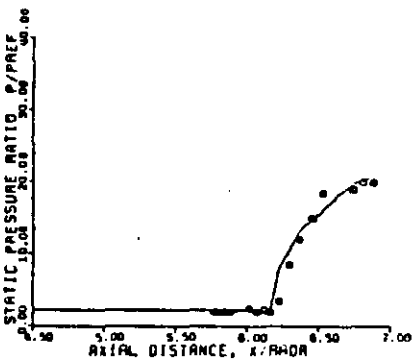

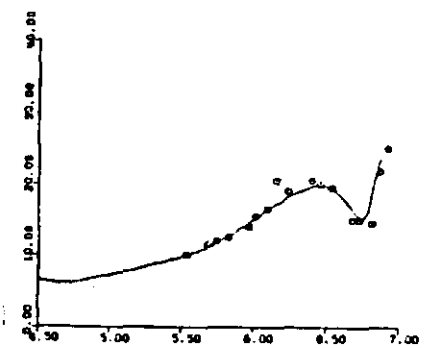

Angle of Attack = +2°

Figure 15. Wall Static Pressure Distribution (-2, 0 and +2 deg)

% difference between inlet mass capture at off-design and design conditions =

captured mass at off design condition - captured mass at design condition

---

captured mass at design conditions

The following important results were obtained:

% difference between inlet mass capture of -2 degrees flow and design conditions (0 degrees) = -15.5%

% difference between inlet mass capture of +2 degrees flow and design conditions (0 degrees)= +11.5%

An interesting observation was made when the mass flow through the inlet was studied from the centerbody leading edge to the beginning of the cowl. For design conditions the mass flow in this region was constant. For the negative angle of attack this mass flow steadily decreased from the leading edge of the centerbody to the beginning of the cowl while for the positive leading edge this mass flow steadily increased.

3. Discussion of the Shock Structure and Strength: The shock structure can be determined from the pressure contours and the plots of centerbody and cowl surface pressures.

Figure 16 shows the effect that varying the angle of attack has on the cowl shock. The inlet outline is shown with the centerbody on the lower surface and the cowl on the upper surface. The grid shows the X/HC values going from 0 to 7. This ratio X/HC gives a measure of the distance in the streamwise direction from the inlet free stream location. HC is the inlet capture height.The cowl starts at a value of 4.4 in this coordinate system. Only the important contours that show the various shock waves have been plotted. The

vertical lines are included to form a grid that helps to locate the position of shock impingement.

It is seen that as the angle of attack goes from +2 to -2 deg the point of impingement of the cowl shock on the centerbody goes further upstream. This can also be seen in the surface pressure plots of the centerbody (Fig 15). The point where the pressure suddenly rises is the point of impingement of the cowl shock on the centerbody.This point of sudden pressure change moves upstream as the angle of attack goes from -2 to +2 deg. However, not much change is seen in the ramp shock coming from the centerbody. The entrance Mach number of the +3.2 deg case was greater than the design value of 6.0 and the value for the -3.2 deg case was smaller than the design value of 6.0. Figure 17 shows the comparison of the pressure contours for the three angles.These contours show the effect of angle of attack on the ramp shock. It is seen that as the angle of attack goes from negative to positive the ramp shock moves farther upstream.

The shock strength can be gauged by the rise in static pressure at the point of impingement of the shock. A study of the wall pressure distribution for the centerbody and cowl show that the shock strength of the cowl shock and the reflected shock wave decreases as the angle is changed from -3.2 deg to +3.2 deg. This is verified by the inclination of the shock wave as seen in the pressure contours. As the angle of attack goes from -3.2 to +3.2, the cowl shock is more inclined to the vertical direction. As the shock wave gets more oblique, the strength decreases.

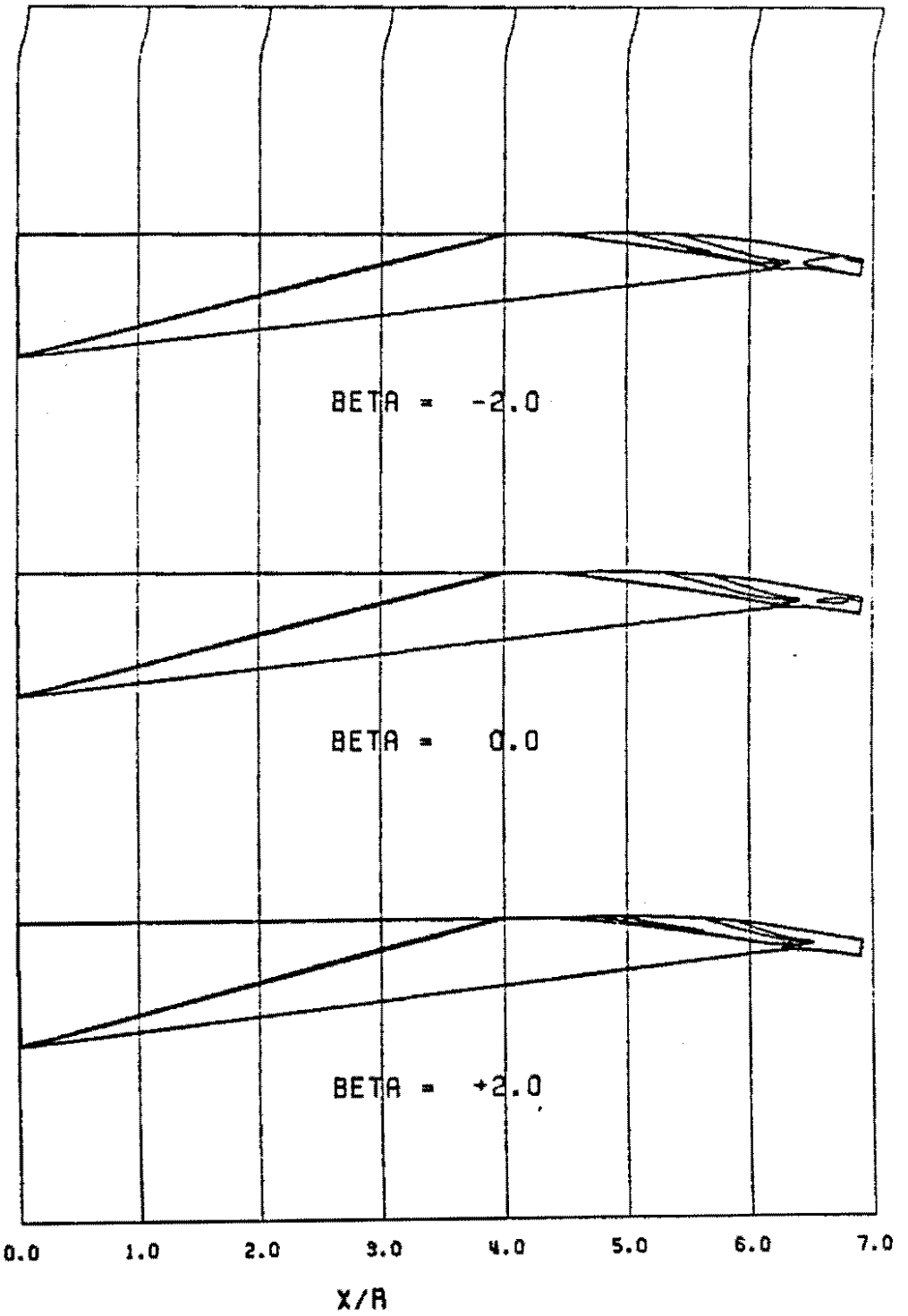

Figure 16. Static Pressure Contours (-2, 0 and + 2 deg)

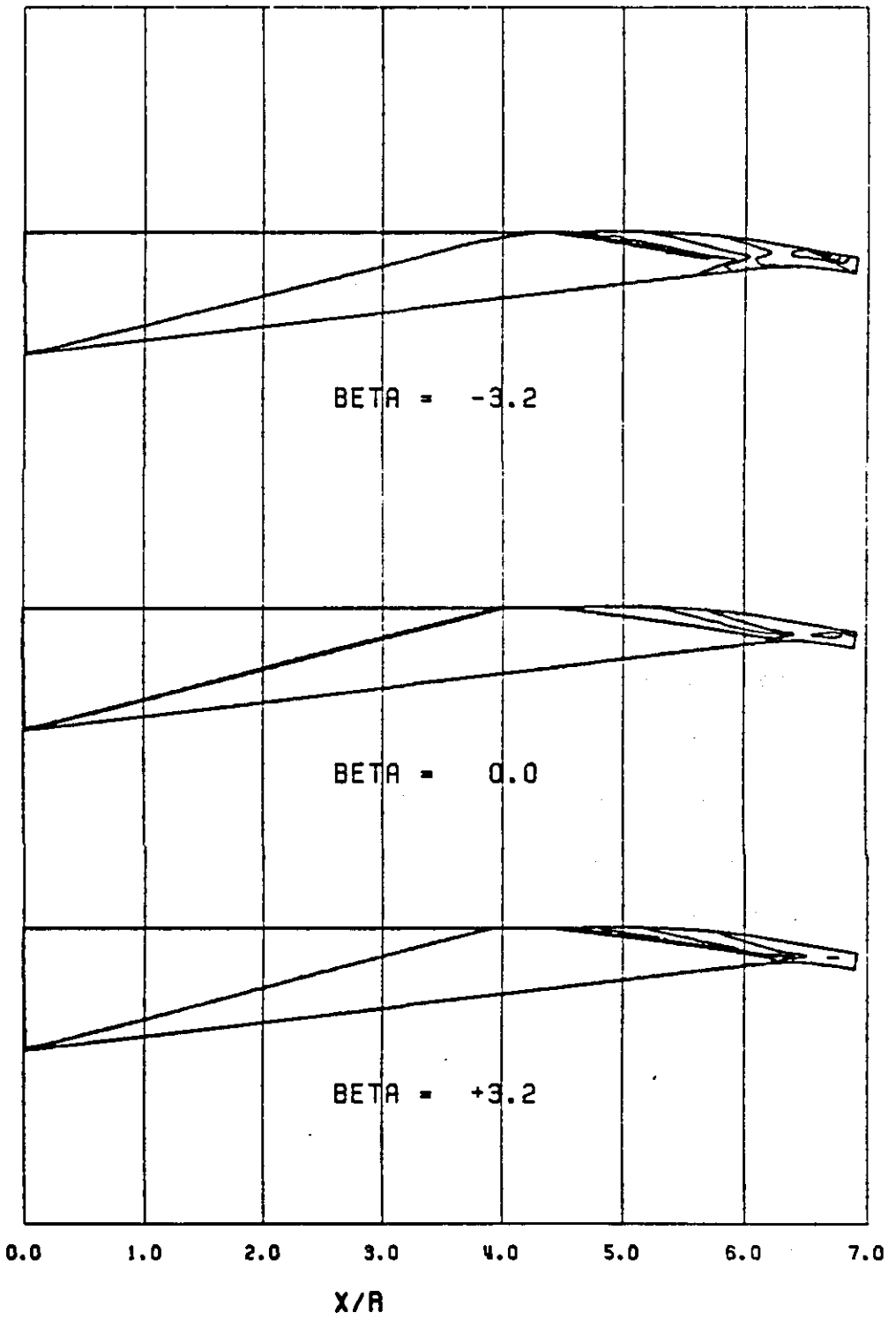

Figure 17. Static Pressure Contours (-3.2, 0 and + 3.2 deg)

4.2.3 The P2 Inlet

The P2 inlet has a compression ratio of 2, unlike the P8 inlet that has a compression ratio of 8. The 3-D calculations of the previous section (4.1) and the variation of the angle of attack in the preceding paragraphs were done on a P8 inlet geometry. As an off-design aspect of the P8 inlet, the P2 inlet was now studied. After modifying the various parameters in the P8 input file, a good match was obtained between the experimental data and the results given by the code. An attempt was made to use the same input parameters with the P2 mesh to see if a good comparison was obtained for the P2 case too.

When the same input file as the P8 one was used, the P2 plots of the pitot pressure did not give a satisfactory comparison. The parameter that specified the boundary layer thickness on the upper and lower surfaces was changed. For the P8 case, it was .07 on both the upper and lower surfaces. For the P2 case a good comparison with the P2 experimental data was obtained when the parameter (DELTAB) was changed to .06 on the upper surface and .05 on the lower surface.

Figure 18 shows the pitot pressure plots of the P2 case.

Though a very close comparison was not obtained on the lower surface, it was most probably because transition was not considered on the lower surface. In actual flow conditions transition takes place on the lower surface. According to the experimental studies[10], for the P2 case there was no transition from laminar to turbulent flow on the upper surface. The flow was laminar all along the cowl surface, right till the throat. However, when the laminar condition was used on the cowl surface a good comparison with experiment was not obtained on the cowl surface. A turbulent boundary layer

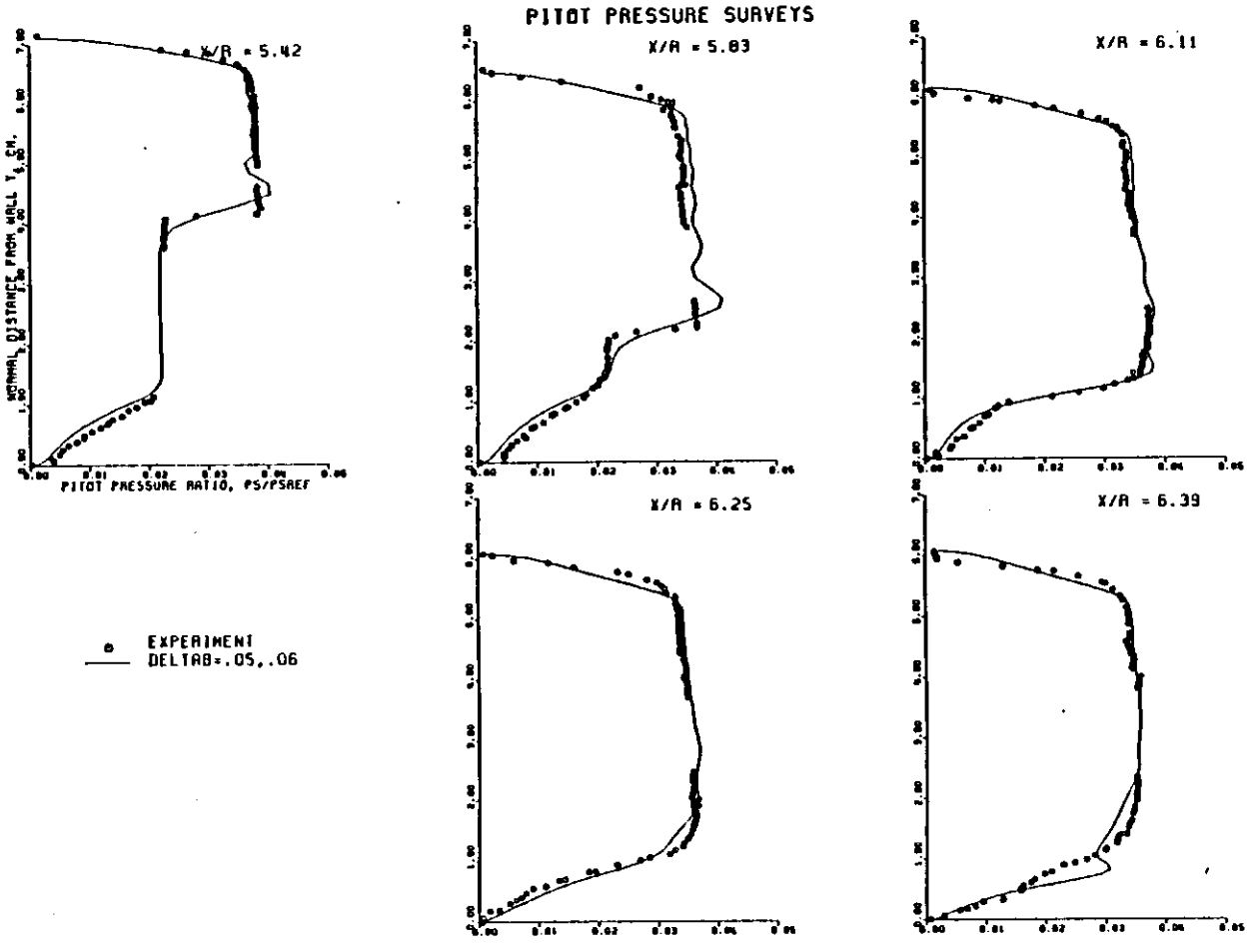

Figure 18. P2 Pitot Pressure Distribution

model with a value of .06 for the boundary layer parameter was the one that gave a good comparison.

Figure 19 shows the cowl and centerbody static pressure plots for the P2 inlet.

Comparison of P8 and P2 pitot and surface pressure profiles. Several interesting observations were made on comparing the pitot pressure profiles of the P8 and P2 inlet.

1. The pitot pressure profiles of the P8 inlet had significant normal gradients.The P2 inlet had relatively small gradients.

2. For the P2 inlet boundary layer edges could not be identified from pitot pressures because of the gradients introduced by the entropy layer generated by the blunt leading edge.

3. The cowl of the P2 inlet did not have shock-wave boundary layer interactions. The P8 inlet experienced this. Hence, in the P8 inlet there was a reduction of surface pressure upstream of the interaction location because of penetration of the cowl shock wave into the thick centerbody boundary layer.

4. The P8 inlet cowl generated a reflected wave after the interaction between the cowl boundary layer and the reflected wave from the centerbody. This reflected wave was the cause of a pressure rise on the cowl surface at a location of about 6.8. The P2 inlet did not have this reflected wave from the cowl. Hence the surface pressure of the cowl did not start to rise .

5. The surface pressures recorded on the cowl and centerbody of the P8 inlet were much larger than similar measurements made with the P2 inlet. The P2 inlet pro-

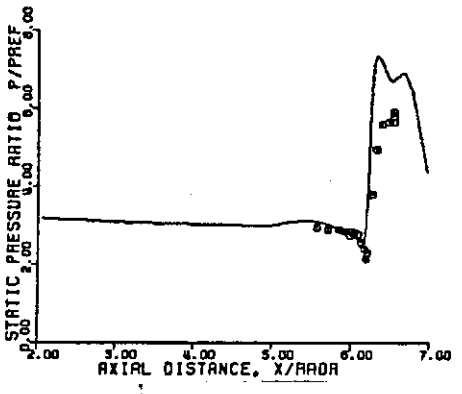

Centerbody

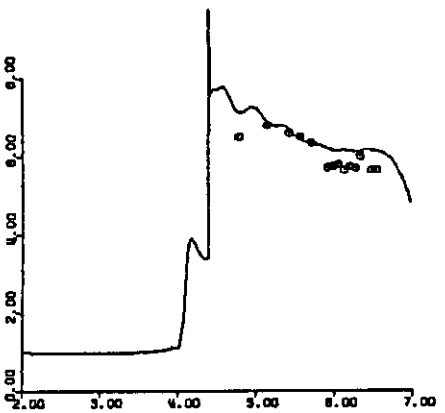

Cowl

Figure 19. Wall Static Pressure Distribution for the P2 Inlet

vided a slight expansion field close to the throat for reasons explained in the introduction. However, in the P8 inlet the cowl curvature near the throat provided added compression and hence caused the pressure to rise.

6. Since the pressure rise was much higher in the P8 inlet, the influence was felt farther upstream. The pressure rise for the P8 inlet began about 1 cm upstream of that for the P2 inlet.

Thus, the set of parameters used in the P8 case cannot be used in the P2 case. The code needs different input parameters for different compression ratios.

5. Conclusions

1. The flow in the P8 inlet was three dimensional but the 3-D effect became prominent only close to the side plates.

2. In the velocity vector and Mach number contours, no significant differences were observed between the straight side plate calculations done at NASA Lewis Research Center and the Cut-back side plate calculations done in this research.

3. No significant differences were observed in the pitot pressure plots of the 2-D and 3-D results.

4. The Lewis Inlet Code could be used for reliable off-design information because a good comparison with the experimental data was obtained.

5. As the angle of attack was changed from negative to positive values, the ramp shock formed a larger angle with the primary streamwise direction and the point of impingement of the cowl shock on the centerbody moved downstream.

6. The shock strength of the cowl shock and its reflection decreased as the angle of attack was changed from negative to positive.

7. Parameters in the input file that gave a good comparison with the experiment for a certain geometry and compression ratio did not give a good comparison with the experiment for a different geometry and compression ratio.

References

1. **Jones, R. A.** and **Huber, P. W.**, "Toward Scramjet Aircraft", *Astronautics and Aeronautics, 1979, pp 38-48.*

2. **Williams, R. M.**, "National Aerospace Plane ", *Aerospace America, Nov.1986, pp 18-22.*

3. "Propelling The Aerospace Plane", *Mechanical Engineering, June 1986, pp 32-36.*

4. **Saad, M.**,"Compressible Fluid Flow", Prentice Hall Inc., Englewood Cliffs, New Jersey, 1985.

5. **Hearth, D. P.** and **Preyss, A.E.**, "Hypersonic Technology-Approach to an Expanded Program", *Astronautics and Aeronautics, Dec 1976, pp 20-37.*

6. "Numerical Aerodynamic Simulation", *NASA.*

7. **White, M. E., Drummond, J. P.**, and **Kumar, A.**, "Evolution and Status of CFD Techniques for Scramjet Application", *AIAA-86-0160, 1986.*

8. **Gnos, A. V., Watson, E. C., Seebaugh, W. R.**, and **Sanator, R. J.**, "Investigation of Flow Fields Within Large-Scale Hypersonic Inlet Models", *NASA TN D7150, 1973.*

9. **Buggeln, R. C., Kim, Y. N.** and **McDonald, H.** "Computation of Multi-Dimensional Viscous Supersonic Flow", *NASA CR-4021, Contract No. NAS3-22027, Oct 1986.*

10. **Anderson, B. H.**, and **Benson,T. J.**, "Numerical Solution to the Glancing Sidewall Oblique Shock Wave / Turbulent Boundary Layer Interaction in 3-D", *AIAA 83-0136.*

11. **Seebaugh, W. R.**, "Hypersonic Flows in Large-Scale Inlet Models", *J.Aircraft, vol.10, no.1., 1973.*

12. **Kunik, W. G., Benson, T. J., Ng, W. F.**, and **Taylor, A.** , "Two- and Three-Dimensional Viscous Computations of a Hypersonic Inlet Flow", *AIAA 25th Aerospace Sciences Meeting, Jan12-15, 1987.*

13. Kumud, A., "Turbulence Modeling in Hypersonic Inlets", Master of Science Thesis, Dept. of Mechanical Engineering, VPI & SU, 1987.

Appendix

A. PLOTTING TECHNIQUES

Velocity Vectors

To make a meaningful interpretation of all the numbers given out as output from the 3-D run plotting techniques are essential.

Secondary velocity vectors are the vectors in the YZ plane showing the V and W components of velocity. They were plotted using the Graphical Kernel System (GKS).Two dimensional data can be processed by this software to give a graphical representation. Given the Y and Z location of the point at which the velocity vector was to be plotted and the V and W components of velocity, an arrow could be drawn. The tail coincided with the location specified and the head was at a point such that the length of the arrow represented the magnitude of the resultant velocity and the direction of the arrow represented the direction of the resultant velocity.

These arrows were also used to represent the 2-D flow field and were used for an animation sequence to help visualize the flow field.

Contours

Contours were plotted using VERSATEC on an IBM VM/CMS system.

B. 2D INPUT FILE FOR THE P8 INLET

```
 P8 W/ OPT 3
2       1.0
&REST
ICOMP=4,IRSTOT=960,IWR=1,
NFILE=0,IRSTIN=0,
NSAVED=0,
&END
&LIST1
IBOUND(1)=2,2,2,2,
IEQBC(1,1)=2,2,2,2,
IEQBC(1,2)=2,2,2,2,
IEQBC(1,3)=2,2,3,2,
IEQBC(1,4)=16,16,16,16,
IEQBC(1,5)=8,8,8,8,
JEQBC(1,1)=11,12,11,11,
JEQBC(1,2)=2,12,11,11,
JEQBC(1,3)=11,12,2,2,
JEQBC(1,4)=14,12,14,14,
JEQBC(1,5)=11,11,17,11,
ASW(1)=.97,
ASW(2)=5.40,
IHSTAG=1,
TWALL=4.24,4.24,4.24,4.24,
IOPTYZ=42*1,
```

```
&END
&LIST2
GAMMA=1.39,
PR=0.71,PRT=0.90,
MINF=7.4,PZERO=4140000.,TZERO=811.,
LREF=.18274,
&END
&LIST3
INH12=0,INH21=0,
TT1(1)=-.99,TT2(1)=.99,TT2(2)=.99,
TWOD=.TRUE.,
IGEOM=10,YS(2,2)=1.0,
NE(1)=99,NE(2)=1,NS=960,
DELX=.00075,XENTR=.11,
IAP=1,300,500,700,6*10000,
AP=1.0,5.0,.2,5.0,1.0,5*1.0,
DXMIN= .0001,.0001,.0002,.0001,6*.000001,
DXMAX=2*.0015,2*.001,5*.01,
&END
&LIST4
AMACRT=1.1,
IWALF=0,IOPTWF=0,
IPRTE=2,IFLARE=1,
ICONS=3,3,1,3,3,1,3,3,1,3,3,1,3,3,1,3,3,1,3,3,1,
IPROF=1,
CRITU=0.05,
AVISC=14*0.00,
```

```
IMIXL=1,
BETA=+2.0,
IVISC=3,DELTAB(1)=.07,.07,.07,.07,
&END
&LIST5
IPLOT=5,
IPRINT=50,
ISW=1,
IVARPR(23)=1,
JWR=5*2,
&END
```

C. 2D INPUT FILE FOR THE P2 INLET

```
 P2 TEST CASE
2       1.0
&REST
ICOMP=4,IRSTOT=300,IWR=1,
NFILE=0,IRSTIN=0,
NSAVED=0,
&END
&LIST1
IBOUND(1)=2,2,2,2,
IEQBC(1,1)=2,2,2,2,
IEQBC(1,2)=2,2,2,2,
IEQBC(1,3)=2,2,3,2,
IEQBC(1,4)=16,16,16,16,
IEQBC(1,5)=8,8,8,8,
JEQBC(1,1)=11,12,11,11,
JEQBC(1,2)=2,12,11,11,
JEQBC(1,3)=11,12,2,2,
JEQBC(1,4)=14,12,14,14,
JEQBC(1,5)=11,11,17,11,
ASW(1)=.97,
ASW(2)=5.40,
IHSTAG=1,
TWALL=4*4.24,
IOPTYZ=42*1,
```

```
&END
&LIST2
GAMMA=1.390,
PR=0.71,PRT=0.90,
M1NF=7.4,PZERO=4140000.,TZERO=811.,
LREF=.18274,
&END
&LIST3
INH12=0,INH21=0,
TTI(1)=-.99,TT2(1)=.99,TT2(2)=.99,
TWOD=.TRUE.,
IGEOM=10,YS(2,2)=1.0,
NE(1)=99,NE(2)=1,NS=300,
XENTR=.11,DELX=0.00075,
IAP=1,300,500,700,6*10000,
AP=1.,5.0,.2,5.0,1.0,5*1.0
DXMIN=.0001,.0001,.0002,.0001,6*.000001,
DXMAX=2*.0015,2*.001,6*.01,
&END
&LIST4
AMACRT=1.1,
IWALF=0,IOPTWF=0,
IPRTE=2,IFLARE=1,
ICONS=3,3,1,3,3,1,3,3,1,3,3,1,3,3,1,3,3,1,3,3,1,
IPROF=1,
CRITU=0.05,
AVISC=14*0.00,
```

```
IMIXL=1,
IVISC=3,DELTAB(1)=.05,.06,.07,.07,
&END
&LIST5
IPLOT=5,
IPRINT=50,
ISW=1,
IVARPR(23)=1,
JWR=5*2,
&END
```

D. Mass Flow Calculations

The grid shown in Figure 18 helps to explain how the mass flow was calculated.

$$M = pAV$$

where M = mass flow

p = density

A = area of cross section

V = velocity of flow

A,B,C,D show the different X locations and 1,2,3,4 show the Y locations for each X location.

For every X location, mass flowing through that position was considered as the summation of the mass flow through 1-2,2-3,3-4 etc.

Considering grid 1-2, the average of the pressures and the average of the temperatures at locations 1 and 2 were taken. From these two averages the average density for the grid 1-2 was determined.

The area of the grid was equal to the Y value of point 1 subtracted from the Y value of position 2 and then multiplied by the depth in the Z direction.

The average streamwise velocity was determined too.

Using formula 1 the mass flow for each small grid was determined.

Using the summation of the mass flows across all the small grids at a particular X location, the mass flow through the the cross section at a particular X location was detemined.

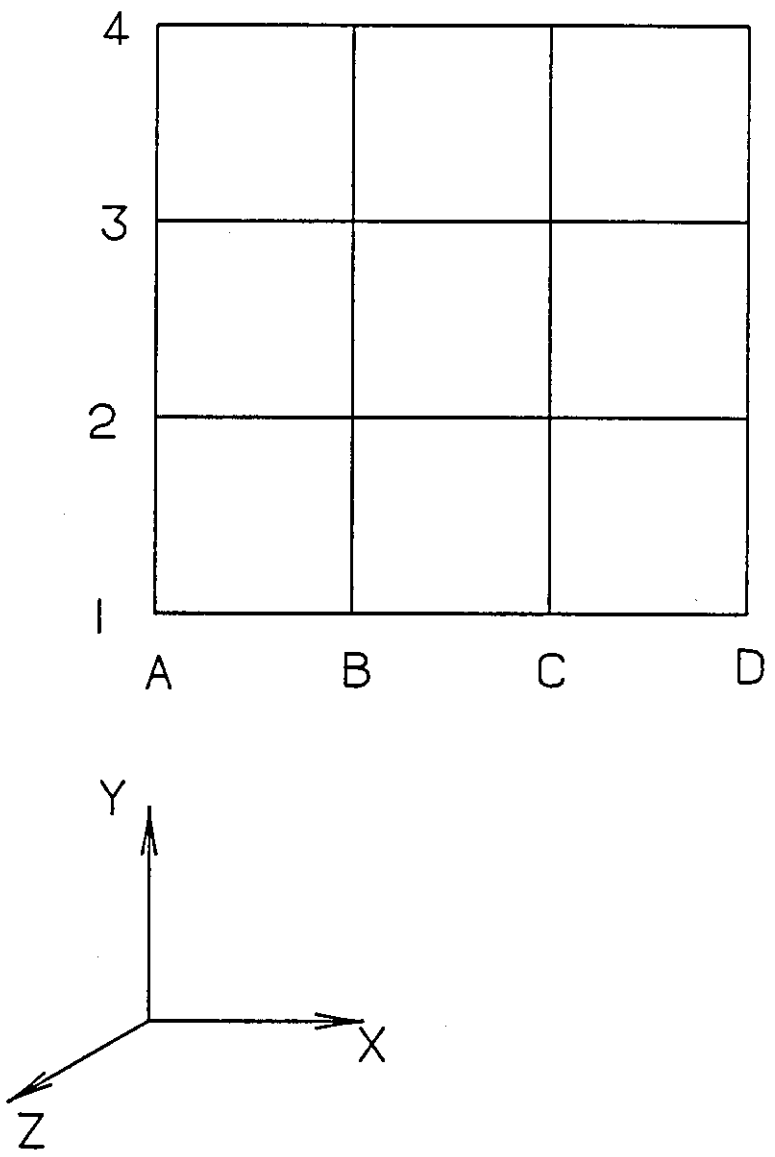

Figure 20. Grid to Show Calculation of Mass Flow

E. Equations Used

The fluid dynamic laws of mass, momentum and energy conservation are as follows [9] :

$$\nabla \cdot \rho \vec{v} = 0 \qquad [1]$$

$$\nabla \cdot (\rho \vec{v} \ \vec{v}) + \nabla P - \frac{\nabla \cdot \tau}{Re} = 0 \qquad [2]$$

$$\nabla \cdot (\rho h_o \vec{v}) - \nabla \cdot [\frac{C_p}{Re}(\frac{\mu_l}{Pr_l} + \frac{\mu_T}{Pr_T})\nabla T] - \nabla \cdot \frac{(\tau \cdot \vec{v})}{Re} = 0 \qquad [3]$$

The stagnation enthalpy is related to the static temperature and velocity by the following relationship

$$H_o = C_p T + \frac{\vec{v} \cdot \vec{v}}{2} \qquad [4]$$

For a perfect gas, the temperature T, pressure P and density ρ are related by the equation of state

$$P = \frac{\gamma - 1}{\gamma} C_p \rho T \qquad [5]$$

These equations are applicable to both laminar and turbulent viscosities when the effective viscosity is considered to be the sum of laminar and turbulent viscosities.

$$\mu = \mu_T + \mu_L \qquad [6]$$

Using the approximations of the Parabolized Navier Stokes' equation (PNS), the reduced forms of equations 2 and 3 are :

$$\nabla \cdot (\rho \vec{v} \quad \vec{v} \quad) + \nabla P - (\frac{\nabla \cdot \tau}{Re})_R = 0 \qquad [7]$$

$$\nabla \cdot (\rho h_o \vec{v} \quad) - \{\nabla \cdot [\frac{C_p}{Re}(\frac{\mu_e}{Pr_e} + \frac{\mu_T}{Pr_T})\nabla T]\}_R - [\nabla \cdot \frac{(\tau \cdot \vec{v} \quad)}{Re}]_R = 0 \qquad [8]$$

where the subscript R refers to the approximated or reduced form of the term.

Attention Patron:

The one-page vita has been removed

from the scanned document